ADVANCED BIOSYSTEMS
www.adv-biosys.com

Biopolymeric Coacervate Microvectors for the Delivery of Functional Proteins to Cells

Wenjin Xiao, Monika D. Jakimowicz, Ioannis Zampetakis, Sarah Neely, Fabrizio Scarpa, Sean A. Davis, David S. Williams, and Adam W. Perriman**

The extent to which biologic payloads can be effectively delivered to cells is a limiting factor in the development of new therapies. Limitations arise from the lack of pharmacokinetic stability of biologics in vivo. Encapsulating biologics in a protective delivery vector has the potential to improve delivery profile and enhance performance. Coacervate microdroplets are developed as cell-mimetic materials with established potential for the stabilization of biological molecules, such as proteins and nucleic acids. Here, the development of biodegradable coacervate microvectors (comprising synthetically modified amylose polymers) is presented, for the delivery of biologic payloads to cells. Amylose-based coacervate microdroplets are stable under physiological conditions (e.g., temperature and ionic strength), are noncytotoxic owing to their biopolymeric structure, spontaneously interacted with the cell membrane, and are able to deliver and release proteinaceous payloads beyond the plasma membrane. In particular, myoglobin, an oxygen storage and antioxidant protein, is successfully delivered into human mesenchymal stem cells (hMSCs) within 24 h. Furthermore, coacervate microvectors are implemented for the delivery of human bone morphogenetic protein 2 growth factor, inducing differentiation of hMSCs into osteoprogenitor cells. This study demonstrates the potential of coacervate microdroplets as delivery microvectors for biomedical research and the development of new therapies.

1. Introduction

Due to their low cytotoxicity, high specificity, and activity, protein-based biologics are a rapidly expanding class of therapeutic agents and are being developed for medical oncology and tissue regeneration.[1–5] Although protein therapeutics have exceptional potential for next-generation therapies, delivery of these macromolecules is hindered due to their vulnerability to biological deactivation,[6–9] poor native membrane permeability, and short circulation time if utilized intravenously.[10–12] For these reasons, the development of protein delivery technologies is a vital endeavor that promises to unlock the potential of this significant class of bioactive macromolecules.[13,14]

An emerging strategy to address the challenge of protein delivery is via the use of coacervate particles, which is appealing due to their ability to spontaneously sequester various macromolecular cargoes,[15,16] and to undergo direct cellular interactions.[17] In these terms, coacervates have been described as biomimetic microcontainers due to their physicochemical semblance to the cell cytoplasm, albeit without an external membrane.[18,19] Although being a relative newcomer to the field of therapeutic protein delivery, coacervate-based materials have received significant attention in biomedical research and have already been used for drug delivery.[20,21] For example, coacervate-based materials have shown great promise for controlled growth factor delivery in vivo for attenuation of disc degeneration, persistent angiogenesis, preservation of

Dr. W. Xiao, Dr. M. D. Jakimowicz, S. Neely, Dr. D. S. Williams, Prof. A. W. Perriman
School of Cellular and Molecular Medicine
University of Bristol
Bristol BS8 1TD, UK
E-mail: d.s.williams@bristol.ac.uk; chawp@bristol.ac.uk

Dr. M. D. Jakimowicz, Dr. S. A. Davis
Bristol Centre for Functional Nanomaterials
University of Bristol
Bristol BS8 1FD, UK

The ORCID identification number(s) for the author(s) of this article can be found under https://doi.org/10.1002/adbi.202000101.

DOI: 10.1002/adbi.202000101

Dr. M. D. Jakimowicz
HH Wills Physics Laboratory
University of Bristol
Bristol BS8 1TL, UK

Dr. M. D. Jakimowicz
Centre for Organized Matter Chemistry and Centre for Protolife Research
School of Chemistry
University of Bristol
Bristol BS8 1TS, UK

Dr. I. Zampetakis, Prof. F. Scarpa
Bristol Composites Institute (ACCIS)
Department of Aerospace Engineering
University of Bristol
Bristol BS8 1TF, UK

heart function after myocardial infarction and skin regeneration.[22–26] Although such recent studies have demonstrated the physical advantages presented by coacervate-based materials in addressing cells in a specific manner, their development toward drug delivery applications is, as of yet, significantly underexplored.

From a practical perspective, the ability to spontaneously assemble coacervates in aqueous solutions that actively sequester protein payloads is a major advantage of this technology. As this technology moves into the biomedical space, however, rationally designed coacervate systems with predictable and tunable behaviors need to be developed in order to identify the physicochemical determinants of therapeutic performance. Two key physical factors underpinning coacervate performance are composition and stability in biological environments. Accordingly, coacervates that can be engineered from biopolymeric building blocks benefit from inherent biocompatibility and their structure can be readily tailored by simple chemical modifications to ensure greater stability under, for example, physiological conditions (high salt and near neutral pH).[27–29] In particular, the use of polysaccharides as a building block for therapeutic technologies exemplifies this logic,[30] and functionalization through derivatization has been described as a biocompatible route toward the development of bioactive materials.[31] Recently, coacervates upon amylose derivatives have been utilized as a platform for the engineering of hierarchical protocells, which present biofunctionality and physiological stability.[32,33]

With this in mind, we explore the utility of functionalized amylose-based coacervates as protein-delivery microvectors. We show that the physicochemical properties of amylose coacervate microdroplets can be readily adjusted by simply varying the constituent stoichiometry, leading to microdroplets with either positive or negative surface charge densities. The resulting microvectors are stable under physiological conditions, noncytotoxic and can be used to deliver a range of protein payloads via spontaneous fusion with the plasma membrane of human mesenchymal stem cells (hMSCs). Finally, we demonstrate that the oxygen storage protein myoglobin (Mb) can be delivered into the cytoplasm of hMSCs within 24 h, and that microvectors loaded with bone morphogenetic protein 2 (BMP2) drove in vitro differentiation of hMSCs into osteoprogenitors. Thus, our amylose-based coacervate microdroplets can be suitable for a range of drug delivery applications, including in vivo localized delivery.

2. Results and Discussion

In previous work, we demonstrated that complex coacervate microdroplets comprising poly(diallyldimethylammonium chloride) and adenosine triphosphate (ATP) could be directly manipulated using optical tweezers to deliver molecular payloads without undermining cellular integrity or function.[17] Although this microdroplet system represented a step in the right direction for coacervate-based vector development, it utilized an industrially derived synthetic polymer and had only moderate droplet stability in cell media. Accordingly, here we look to develop the versatility of coacervate microdroplets and explore the principal physicochemical factors that determine their performance *in cellulo*. Critical factors in the utility of coacervates for cell-based therapies are their biocompatibility, stability under physiological conditions, such as ionic strength, and the ability to deliver functional payloads to and across the plasma membrane.[21]

2.1. Synthesis and Physical Characterization of the Coacervate Microvector

Capturing developments in the area of synthetic cellularity and reapplying them in a biomedical context is something of a cycle in the conceptual evolution of bioinspired materials. The advantage of using synthetically functionalized biopolymer components for the fabrication of coacervate microdroplets is the ability to tune their stability by systematically modifying charge density, which will affect the "stickiness" by modulating the magnitude and frequency of electrostatic interactions (both internally and externally). Synthetic coacervate microdroplets comprising modified amylose (a linear biopolymer) provides an exciting platform that can be applied to the controlled delivery of macromolecular cargos to cells. Having been established as a technology for the engineering of biocompatible synthetic protocells, amylose-coacervates have demonstrated enhanced stability under increased ionic strength.[33] Accordingly, the components for complex coacervate microdroplets of both quaternized amylose (QA) or carboxymethylated amylose (CMA) variants, with positive or negative charges, respectively, were synthesized upon modification of amylose polymer using a protocol adapted from Amar-Lewis et al.[34] (**Figure 1**). Here, coacervate microdroplets were formed due to the electrostatic interaction between polyelectrolyte chains, driven by phase separation of the partially neutralized complexes into a polymer-rich (coacervate) state. Having synthesized highly charged amylose derivatives with a degree of substitution (DS) of 1 (QA_1/CMA_1) (Figure S1, Supporting Information), we initially ensured that the phase diagram for coacervate formation was broad enough to generate stable coacervate droplet dispersions over a wide range of QA_1/CMA_1 stoichiometries. Indeed, the coacervate formation, as indicated by the onset of solution turbidity, between QA_1/CMA_1 components was clearly evident in all mixing stoichiometries up to ≈90% (**Figure 2**a). In order to demonstrate its ability to tailor the overall charge of this system, the effect of various stoichiometries was compared upon zeta-potential for the mixture of QA_1 with either CMA_1 or half-substituted $CMA_{0.5}$ (Figure 2b). As expected, the equally charged mixtures of QA_1/CMA_1 followed an almost sinusoidal curve with zero charge at the equimolar mark that became positively/negatively charged when there was an excess of QA_1/CMA_1, respectively. By contrast, the mixture of QA_1/$CMA_{0.5}$ showed an overall positive charge over the entire mixing range, due to the chemically programmed charge imbalance between the two components.

In order to favorably interact with anionic sulphated proteoglycans on the cell plasma membrane, the coacervate microdroplets need to be engineered to exhibit positive surface charge density at pH 7.3. Thus, the cationic coacervate microdroplets comprising QA_1/$CMA_{0.5}$ of 1:1 and 2:1 volume ratios were readily prepared in solution, respectively. These coacervate

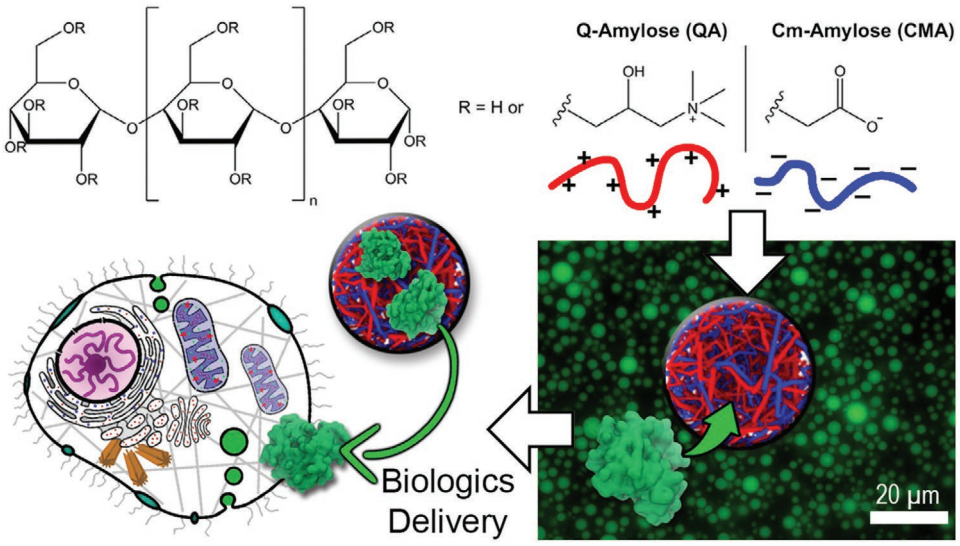

Figure 1. Schematic outlining the chemical composition of amylose-based, biopolymeric coacervate microdroplets, and their ability to spontaneously sequester biologic cargos, transporting them to cells as a new mode of therapeutic protein delivery.

microdroplets were assessed for their stability under physiological conditions in terms of temperature and ionic strength. The stability of coacervate microdroplets comprising $QA_1/CMA_{0.5}$ of 1:1 was not undermined at the elevated temperature of 37 °C, however, the 2:1 stoichiometry did show a reduction in turbidity (Figure S2a, Supporting Information). It is crucial to generate coacervate complexes with positive charges upon introducing the two components of 1:1 ratio, as such balance of charges within the coacervate complex would allow for simultaneous preservation of sufficient charged sites on each component, to ensure high stability of the complex when interacting with the cell membrane in presence of other charged species, such as salts. This was demonstrated using coacervate microdroplets comprising $QA_1/CMA_{0.5}$ of 1:1, which maintained highly stable in cell media at the physiological ionic strength (Figure S2b, Supporting Information). Accordingly, a $QA_1/CMA_{0.5}$ of 1:1 was used for all the subsequent studies. These stable microdroplets were of size around 1–5 μm (average 2–2.5 μm, Figure 2c).

2.2. Protein Sequestration Capacity of the Coacervate Microvector

The ability of coacervate microdroplets to actively sequester macromolecular cargos is a key facet of its interest as a model protocell and is a significant mechanism by which this structurally complex phase of matter can be imbued with higher-order functionality.[16,23–25,35–39] The capacity of our coacervate microdroplet system to sequester protein payloads of different sizes and charges was next explored and the impact of this on droplet stability, charge and size was also studied. Three functional protein models were selected in this study: enhanced green fluorescent protein (eGFP, MW = 30.7 kDa, pI = 6.26) and cationized enhanced green fluorescent protein (cGFP, MW = 32.5 kDa, pI = 10.40), both for cell labeling and tracking; and myoglobin (Mb, MW = 16.9 kDa, pI = 6.97) labeled with *N*-hydroxy-succinimidyl (NHS)-fluorescein isothiocyanate (FITC), which can facilitate oxygenation and detoxification of cells (Figure S3, Supporting Information).[40] The coacervate microdroplets were formed as evident via transmitted light detection, and the spontaneous sequestration of all three proteins into the coacervate phase was observed (**Figure 3**a). The distribution of proteins was homogenous throughout the coacervate microdroplets, though some aggregation of cGFP was observed as well as the high background fluorescence, which signified lower levels of partitioning. This observation was supported by evaluating protein-coacervate partition coefficients, which were 1200 (± 500) for eGFP, 10 (± 3) for cGFP and 35 (± 11) for Mb, respectively (Figure 3b). The affinity of the protein components with the coacervate could be understood from the zeta-potential values of the individual components (Figure S4a, Supporting Information), whereby the highly positively charged QA_1 would strongly interact with $CMA_{0.5}$, eGFP, and Mb that were all negatively charged and $CMA_{0.5}$ would interact with positively charged cGFP. Protein loading into the coacervates altered the droplet zeta-potential except for Mb (Figure S4b, Supporting Information) and all the coacervate microdroplets, regardless of the charges of proteins sequestered, maintained positive surface potential. A small increase in the average diameter of coacervate microdroplets was observed after sequestration of all three proteins when compared to the unloaded control (Figure S4c, Supporting Information).

The partitioning coefficient of eGFP did not greatly change with pH, with uptake least effective near the protein pI and increasing by ≈10% at low or high pH values in response the overall charge of the protein, improving interactions with the coacervate phase (Figure S5a, Supporting Information). At elevated ionic strength (particularly above 0.5 M), eGFP was released in a nonlinear manner due to destabilization of the coacervate microphase (Figure S5b, Supporting Information). At least 70% of the eGFP sequestered remained within microdroplets at an ionic strength of 0.18 M, equivalent to that of cell culture media. Interestingly, the release of the sequestered payload (eGFP) from the coacervate phase could be induced by the

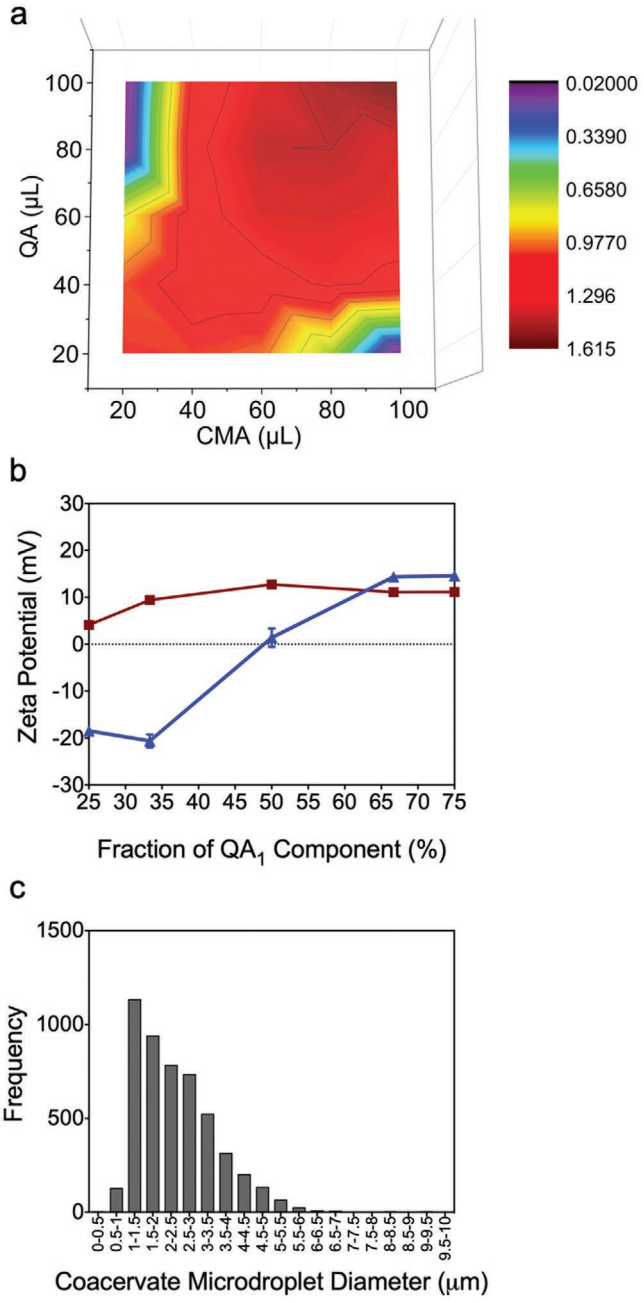

Figure 2. Synthesis and biophysical characterizations of amylose-based coacervate microdroplets. a) A heat map showing the turbidity for varying stoichiometries of two amylose components, quaternized amylose (QA_1) and carboxymethylated amylose (CMA_1) with a degree of substitution of 1. The color bar on the right shows a scale of all colors from the map with their corresponding turbidity value. b) Zeta potential of non-resuspended coacervate systems of QA_1/CMA_1 (blue) and $QA_1/CMA_{0.5}$ (red). The squares and the triangles represent the mean average and the error bars represent the standard deviation ($n = 6$). c) The size distribution of unloaded coacervate microdroplets at room temperature, determined by analyzing acquired widefield images of microdroplets using Fiji software. Both CMA and QA were prepared in Milli-Q water at 1 wt% at pH 7.4.

addition of α-amylase, which was capable of digesting the synthetically modified amylose chains within 3 h at a concentration of 5 U mL^{-1} (Figure S6, Supporting Information), and indicated that the system could be developed for smart vectors with triggered release profiles. The capacity of the coacervate microdroplet system to sequester multiple proteins simultaneously was also investigated. Dual-sequestration ability of eGFP and Mb was observed by confocal microscopy images (Figure S7, Supporting Information). This result showed a feature of our coacervate microdroplet system across a range of complex compositions, with a potential application of delivering a combination of two or three protein-based therapeutics with improved efficacy.[24]

2.3. Interaction of Coacervate Microvector with hMSCs

Having studied the important physicochemical properties of amylose-based coacervates, we then sought to explore their interactions with cells and capacity to deliver protein payloads. The potential cytotoxicity of coacervate microdroplets was estimated by performing cell metabolic assays (3-(4,5-dimethylthiazol-2-yl)-5-(3-carboxymethoxyphenyl)-2-(4-sulfophenyl)-2H-tetrazolium; MTS) on bone marrow-derived hMSCs. Importantly, hMSCs showed no obvious decrease in cell viability (>93.0%) as a result of exposure to most of the individual coacervate components ($QA_1/CMA_{0.5}$), empty coacervate microdroplets or those loaded with protein cargos (eGFP, cGFP, and Mb) (**Figure 4**a). The nontoxicity of this coacervate microdroplet system is expected given the biopolymeric nature of the constituent components.

In order to explore the cellular partitioning of the coacervate components in greater detail, the locations of each individual coacervate component were tracked by fluorescein (FITC) labeling after the delivery, performed 3 and 24 h after introduction of the coacervate microdroplets to hMSCs in media (Figure 4b). The positively charged QA_1 was observed to promptly interact with hMSCs, showing spontaneously membrane binding ability within 3 h and internalization within 24 h after delivery. Conversely, the anionic coacervate component, $CMA_{0.5}$, was found to persist locally at the area of the initial interaction for 24 h. This indicates that the two coacervate components, although they bind strongly enough to withstand the ionic strength of media, dissociate after being in contact with cells for over 3 h—an important property that can facilitate delivery (release) of cargo. No evidence of internalization of either component into nucleus was observed.

2.4. The Delivery of Protein Payloads to hMSCs

As a proof-of-principle experiment for the delivery of functional biologics into the cell, we studied the potential for cellular delivery of coacervate microdroplets loaded with NHS-FITC-labeled Mb (FITC_Mb). Here, the delivery of coacervate-sequestered protein was monitored with live cell imaging at 5 min, 3 and 24 h after introduction of the loaded microdroplets. Free FITC_Mb had no inherent affinity for hMSCs and showed no binding to the plasma membrane (**Figure 5**a). In stark contrast to this, we observed a significant increase in protein localization at the cell membrane after administration of the coacervate delivery system, which reflected the punctuated nature of microdroplet "paintballing" of the cell (Figure 5b). After 3 h FITC_Mb

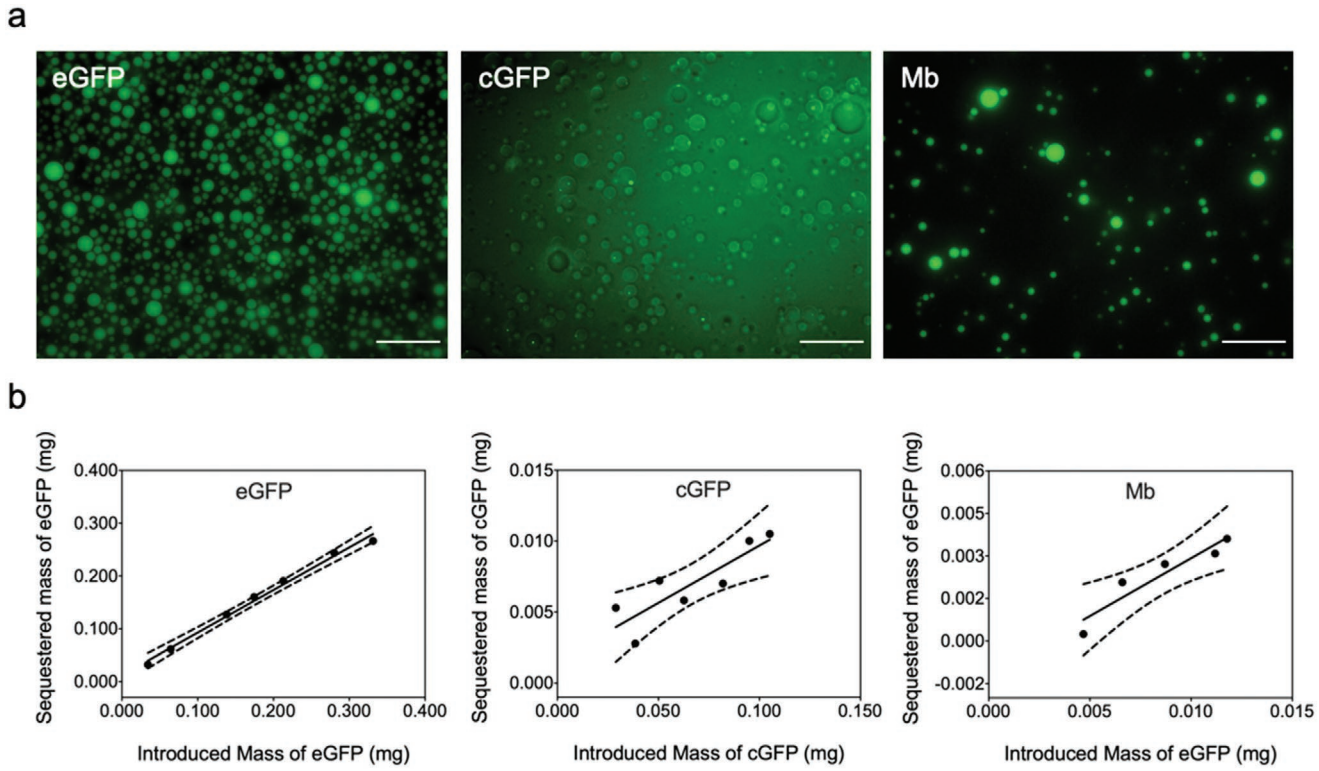

Figure 3. Protein sequestration of coacervate microdroplets. a) Live cell confocal fluorescence microscopy images of sequestered enhanced green fluorescent protein (eGFP, green), cationized enhanced green fluorescent protein (cGFP, green), and myoglobin (Mb, labeled with NHS-FITC, green) in the coacervate microdroplets. Scale bars = 20 µm. b) The sequestration rates for eGFP, cGFP, and Mb, determined by comparing the absorbance of unsequestered proteins in the supernatant to the original solutions using UV–vis spectroscopy. The solid straight line represents the linear regression trend of the data, and the dotted curve on each side of the trend line represents the 95% confidence interval.

began to disperse on the cells with an evidence of internalization into punctuated endosomal structures in a fashion similar to QA but more pronounced (Figure 5c). After 24 h of incubation, the functional protein had been fully internalized by the cells and channeled into endo-lysosomal compartments as indicated by their highly regular, punctuated pattern (Figure 5d). We propose that coacervate-mediated delivery of protein cargo occurred through localized concentration and clustering at the plasma membrane, likely via an endocytic mechanism,[29,41] under the influence of cationic QA that interacts with the anionic outer membrane (cf. Figure 4b). The delivery mechanism is more dependent on the surface charge and stability of the coacervate, rather than the size,[42], i.e., strong interactions with the plasma membrane can deform soft membrane-free coacervate microdroplets.[43] From these results, we can clearly see that the coacervate-mediated delivery of protein cargos provides a substantial increase over the background level of uptake in the solution-phase and the physical control achieved using this method constitutes a major step in the development of new platforms to enable cellular reprogramming.

2.5. Controlled hMSC Differentiation Induced by Coacervate-Sequestered Growth Factor

In light of the effect protein delivery to the plasma membrane and the cytosol, and as a final demonstration of utility for this coacervate microdroplet system, recombinant human BMP2 was partitioned into the coacervate microdroplets and the system tested as a potential microvector for growth factors. BMP2 acts as a master regulator that can induce osteogenic differentiation of hMSCs and stimulate the expression of essential markers at different developmental stages, including osteoblast runt-related transcription factor 2 (RUNX2), an primary osteogenic marker,[44] and alkaline phosphatase (ALPL), an early osteogenic marker.[45] Quantitative analysis of the differentiation potential of coacervate microvectors was assessed via quantitative polymerase chain reaction (qPCR) after a one-week differentiation process. Here, the expression levels of RUNX2 were monitored via comparison with the housekeeping gene glyceraldehyde 3-phosphate dehydrogenase (GAPDH).[46] The 6.8-fold upregulation in expression of RUNX2 showed successful initial differentiation of hMSCs into osteoprogenitors upon exposure to coacervate complexes loaded with 1.7 µg mL^{-1} of BMP2 (**Figure 6**a). A slightly higher 7.8-fold upregulation of RUNX2 was found in the cells exposed to complete differentiation media, which is believed due to a time-dependent effect of cell exposure to BMP2. Since the BMP2 receptors localize at the cell membrane,[47] cells directly exposed to free BMP2 could potentially initialize the differentiation process earlier than those treated with the coacervates, as free BMP2 would diffuse faster in media than the microdroplets, and BMP2 has to also diffuse through the coacervate phase in the microdroplets. Accordingly, the expression of RUNX2, which acts as a primary

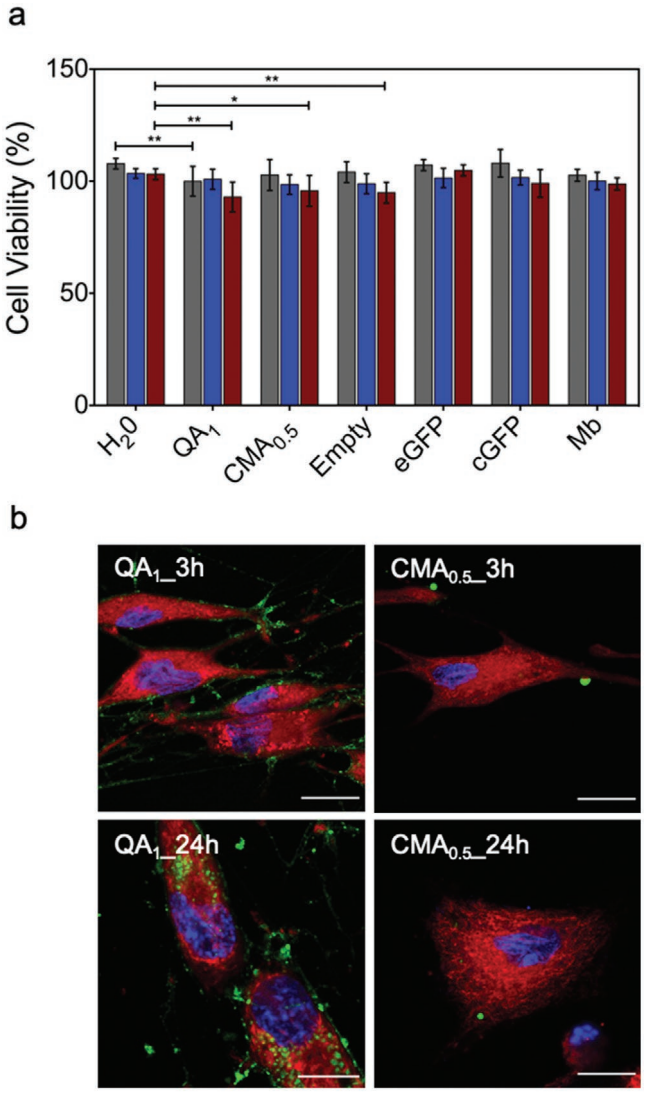

Figure 4. The interaction of coacervate microdroplets with the human mesenchymal stem cell (hMSC) plasma membrane. a) hMSC viability as a function of low (90 microdroplets per cell, 2.5×10^{-3} μg μL^{-1} of $CMA_{0.5}$ or QA_1 (≈0.16×10^{-6}–0.21×10^{-6} M), gray), medium (180 microdroplets per cell, 5×10^{-3} μg μL^{-1} of $CMA_{0.5}$ or QA_1 (≈0.32×10^{-6}–0.42×10^{-6} M), blue), and high (1800 microdroplets per cell, 5×10^{-2} μg μL^{-1} of $CMA_{0.5}$ or QA_1 (≈3.2×10^{-6}–4.2×10^{-6} M), red) incubation concentrations of individual coacervate components and coacervate microdroplets with sequestered proteins, determined by 3-(4,5-dimethylthiazol-2-yl)-5-(3-carboxymethoxyphenyl)-2-(4-sulfophenyl)-2H-tetrazolium (MTS) assay. The bars represent the mean average and the error bars represent the standard deviation calculated using hMSCs from three different patients ($n = 3$). Statistical significance was calculated using a two-way ANOVA test with Bonferroni post-tests. A p-value of less than 0.05 and 0.01 considered significant (*) and highly significant (**), respectively, when compared to the cells treated with H_2O. b) Live cell confocal fluorescence microscopy images showing the cell membrane affinity of FITC-labeled QA_1 (green) or FITC-labeled $CMA_{0.5}$ (green) in hMSCs, respectively, imaged after 3 h post incubation with coacervate microdroplets (with only one component labeled) for 15 min, and after a further 24 h. Cell cytoplasm was stained with a CellTracker Red CMTPX Dye (red) and cell nuclei were stained with a Hoechst dye (blue). Scale bars = 20 μm.

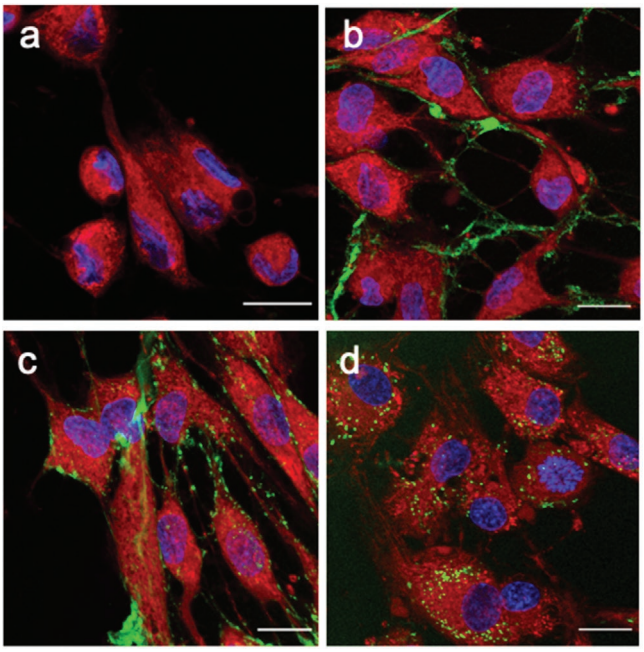

Figure 5. The interaction of protein-loaded coacervate microdroplets with human mesenchymal stem cells (hMSCs) over time. Live cell confocal fluorescence microscopy images showing hMSCs incubated with media containing a) free myoglobin (Mb) after 5 min, or Mb-loaded coacervate microdroplets after b) 5 min, c) 3 h, and d) 24 h. Cell cytoplasm was stained with a CellTracker Red CMTPX Dye (red) and cell nuclei were stained with a Hoechst dye (blue). Mb was labeled with NHS-FITC (green). Scale bars = 20 μm.

transcription regulator of osteogenesis, could be triggered first and accumulated quickly upon the BMP2 treatment.[48,49]

The differentiation indication was further supported with upregulation of both ALPL gene expression (Figure 6b) and protein expression tested using a colorimetric assay (Figure 6c).[50] Here, expression levels of both ALPL gene and protein were significantly increased in the hMSCs exposed to coacervate microdroplets carrying the BMP2 payload when compared to the cells treated with control basal media without BMP2, and comparable to those in the complete differentiation media. Compared to RUNX2, ALPL is a relative later stage osteogenesis marker, the expression of which is regulated by both BMP2 and RUNX2 and highly time-dependent.[48,49] The different expression levels of RUNX2 and ALPL at different time points during osteogenic differentiation process have also been observed by other groups.[51,52]

3. Conclusion

In this work, we rationally designed, built and characterized a novel complex coacervate microvector system for delivering proteins to cells, which spontaneously interacted with the plasma membrane of hMSCs and released the sequestered payloads. This coacervate microdroplet system is stable under physiological pH, ionic strength, and temperature and a range of proteins with different sizes and charges could be successfully sequestered. Particularly, Mb was delivered to the membrane of hMSCs and internalized within the cells. Significantly,

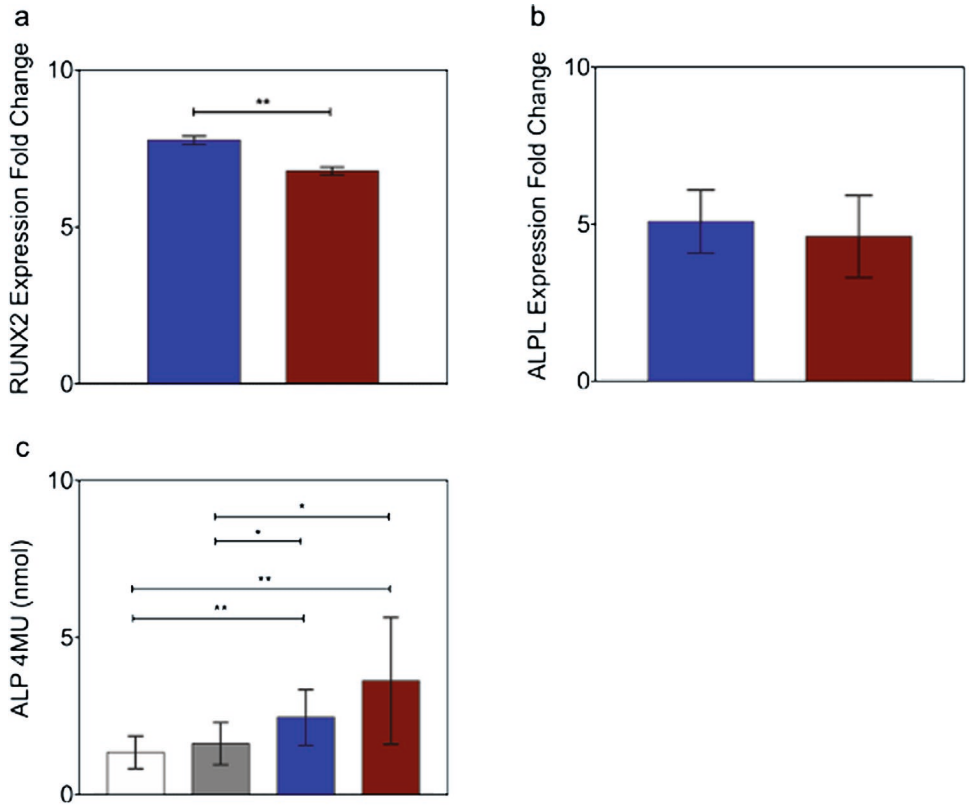

Figure 6. Directed differentiation of the human mesenchymal stem cell (hMSCs) induced by bone morphogenetic protein 2 (BMP2) delivery of coacervate microdroplets. The upregulation in a) runt-related transcription factor 2 (RUNX2) and b) alkaline phosphatase (ALPL) expression of osteoprogenitors induced by treating hMSCs with complete differentiation media supplemented with BMP2 (blue) or coacervate microdroplets with sequestered BMP2 (red) for a week, compared to the cells treated with basal media without BMP2, determined by qPCR. c) The ALP expression of osteoprogenitors induced by treating hMSCs with empty coacervate microdroplets (gray), complete differentiation media supplemented with BMP2 (blue), and coacervate microdroplets with sequestered BMP2 (red) for a week, compared to the cells treated with basal media without BMP2 (white), determined by an ALP assay. The bars represent the mean average and the error bars represent the standard deviation calculated using hMSCs from three different patients ($n = 3$). Statistical significance was calculated using a two-tailed Student's *t*-test. A *p*-value of less than 0.05 and 0.01 considered significant (*) and highly significant (**), respectively.

sequestration of BMP2 into the coacervate system and subsequent cell treatment induced osteogenic differentiation of hMSCs. Accordingly, our coacervate microvector system could be readily adapted to other proteins, regardless of their native affinity to the cell membrane, which could have major implications for biologics development.

4. Experimental Section

Amylose Modification and Characterization: Amylose was purchased from Carbosynth (UK) (MW = 12–16 kDa, n = 74–79) and all other chemicals used for modification purposes were purchased from Sigma-Aldrich (UK) and used without further purification. Q-amylose (QA) with a degree of modification (DM) of 1 (1 modification per anhydrous glucose unit, QA_1) was prepared by dissolving 1.5 g of amylose and 2.1 g of sodium hydroxide in 27 mL of Milli-Q water at 35 °C. After complete dissolution of the amylose, 4 mL of (3-Chloro-2-hydroxypropyl) trimethylammonium chloride (CHPTAC) solution (60 wt% in water) was added dropwise into the stirring reaction mixture, which was subsequently left to react overnight. After the reaction was completed, the mixture was neutralized with acetic acid and precipitated into 200 mL of cold ethanol. The resulting precipitate was redissolved in Milli-Q water and dialyzed extensively against water using regenerated cellulose dialysis tubing (Spectrum Labs, USA) with a molecular weight cut-off (MWCO) at 3.5 kDa.

CM-amylose with a DM of either 1 or 0.5 (CMA_1 and $CMA_{0.5}$) was prepared by dissolving 1.5 g of amylose and 3.6 g of sodium hydroxide in 15 mL of Milli-Q water at 70 °C. After complete dissolution of the amylose, 2.7 g (CMA_1) or 1.8 g ($CMA_{0.5}$) of chloroacetic acid was added and the reaction mixtures were left to stir for 2 h. After the reaction was completed, the mixture was neutralized with acetic acid and precipitated into 200 mL of cold ethanol. The resulting precipitate was redissolved in Milli-Q water and dialyzed extensively against water using regenerated cellulose dialysis tubing with a 3.5 kDa MWCO (Spectrum Labs, USA), and freeze-dried.

NMR Spectroscopy: ^{1}H-NMR spectroscopy measurements were carried out to assess the DS. Samples were dissolved in the Milli-Q water at a concentration of 20 mg mL^{-1} and loaded into quartz NMR tubes. Proton NMR data were collected on a Varian 400 NMR spectrometer (Agilent technologies, UK) at 25 °C with 32 scans and a relaxation delay of 5 s, and the spectrum was integrated to find number of amylose, acetate group, and CHPTAC protons.

FITC Labeling QA and CMA: FITC-labeled QA and CMA were synthesized by dissolving either component in Milli-Q water with 5% NaOH and five equivalents of FITC to react with the hydroxyl groups on the polymers at high pH overnight. After this time, the solution was precipitated into ethanol and then dialyzed extensively.

Coacervate Preparation: CMA and QA were both prepared in Milli-Q water at 1 wt%. Both stock solutions were found to have pH of 7.4. The

coacervate phase was synthesized by combining equivalent volumes of each polymer solutions and Milli-Q water. Any payload materials to be sequestered into the coacervate system were introduced at desired concentrations in place of Milli-Q water. The system was and vortexed for 10 s and subsequently isolated by centrifugation at 4300 RCM for 5 min into coacervate bulk phase and removal of supernatant. Coacervate pellet was resuspended in Milli-Q water by vortexing for 30 s, creating more stable coacervate microdroplets and removing any uncomplexed components. The final concentration of 8.3×10^{-12} µg per microdroplet was calculated for each polymer.

Coacervate Microdroplet Turbidity: The turbidity of the solution upon formation of complex coacervates was assessed by measuring absorbance (A) at 500 nm using UV–vis spectrophotometry, which was directly proportional to the scattering caused by turbid solutions. Collected absorbance readings were converted to corresponding turbidity using Equations (1). The turbidity for a range of stoichiometries was obtained by varying volumes of QA and CMA independently of each other between 0 and 100 µL with Milli-Q water added to make the volume up to 300 µL. Similarly, the stability of coacervate microdroplets was assessed in a range of media concentrations, using Dulbecco's modified Eagle's medium in place of Milli-Q water

$$\%T = 100 \times 10^{-A}$$
$$\text{Turbidity} = 100\% - T\% \quad (1)$$

Protein Expression and Purification: eGFP was expressed in house, using BL21 competent *Escherichia coli* (New England Biolabs, USA)., transformed with the plasmid vector pET45b(+) (Novagen, Germany). The transformed *E. coli* was introduced in 10 mL of lysogeny broth (LB) with 10 µL of 50 mg mL^{-1} carbenicillin (Apollo Scientific, UK) for a starter culture. The sample was incubated overnight at 37 °C and stirred at 180 RPM in a shaking incubator. The resulting culture was added to 1 L of LB medium with 1 mL of 50 mg mL^{-1} of carbenicillin and incubated at 37 °C with 200 RPM for 2 h. Bacterial growth was monitored using UV–vis spectrometer by measuring optical density (OD) at $\lambda = 600$ nm, until it reached 0.6–0.8. Protein expression was induced using 1 mL of 1 M isopropylthiogalactosidase (Apollo Scientific, Japan) and the culture was subsequently incubated at 30 °C for 4 h, followed by a reduction of temperature to 16 °C for overnight expression. The cells were centrifuged at 4500 RCF for 35 min using a Sorvall RC6 Centrifuge (Thermo Scientific, UK).

The resulting cell pellet from each 1 L culture was resuspended in 50 mL lysis buffer containing 50×10^{-3} M NaH_2PO4, 300×10^{-3} M NaCl and 10×10^{-3} M imidazole adjusted to pH 8, followed by addition of 50 µL of 0.1 M phenylmethylsulfonyl fluoride (PMSF) solution, a protease inhibitor. The lysis of the cells was performed using Polytron PT25000 homogenizer (Kinematica, Germany) to release the contents of the cells into solution. After homogenisation, a further 50 µL of 0.1 M PMSF solution was added to the solution. The resulting lysate was centrifuged at 20 000 RCF for 40 min to remove cell debris. The supernatant was purified using a nickel–nitrilotriacetic acid (Ni–NTA) resin column, and the protein was eluted using an elution buffer consisted of 50×10^{-3} M NaH_2PO_4, 300×10^{-3} M NaCl, and 250×10^{-3} M imidazole at pH 8, and was subsequently dialyzed into 20×10^{-3} M phosphate buffer using 12–14 kDa MWCO dialysis tubing (Medicell International, UK). Finally, the purity was assessed using sodium dodecyl sulfate polyacrylamide gel electrophoresis.

Mass Spectrometry: Matrix-assisted laser desorption ionization time of flight mass spectrometry (Bruker, UK) was used to determine the mass to charge ratio of proteins. 2,5-dihydroxyacetophenone matrix was prepared by mixing 20 mg mL^{-1} of 2,4-dihydroxyacetophenone in ethanol with diammonium hydrogen citrate at a 3:1 volume ratio. To prepare an saturated solution of sinapinic acid, 1 mL of matrix solution containing a volume ratio of 70:30 water:acetonitrile with 0.1% trifluoroacetic acid was added to 20 mg of sinapinic acid. The protein was mixed at a 1:1 volume ratio with either of the matrices, of which 2 µL was deposited onto a ground steel sample plate and allowed to air-dry. Multiple spectra were additively acquired between 10 and 50 kDa using FLEX Control software (Bruker, USA) and peaks in the spectra were identified using Origin software (OriginLab Corporation, USA).

eGFP Cationization: 5 mg mL^{-1} eGFP was added to 100 mg mL^{-1} of *N*,*N*′-dimethyl-1, 3-propanediamine at pH 7. The solution was stirred for 4 h at pH 6.9, followed by addition of *N*-(3-Dimethylaminopropyl)-*N*′-ethylcarbodiimide hydrochloride, and finally left to stir for another 24 h at pH 6.6. The product was dialyzed into 20×10^{-3} M phosphate buffer.

Fluorescein Labeling of Myoglobin: NHS-FITC was prepared to a concentration 10 mg mL^{-1} in dimethyl sulfoxide and introduced in excess to myoglobin in HEPES buffer, at pH 7. The solution was incubated for 1 h at room temperature. Any nonreacted NHS-FITC was removed using Zeba spin desalting columns with a 7 kDa MWCO (Thermo Fisher, USA), which utilizes size-exclusion chromatography resin. The final product, NHS-FITC-labeled myoglobin (FITC_Mb), was stored in 20×10^{-3} M HEPES buffer, at pH 7 at −20 °C.

Protein Sequestration Efficiency: The supernatant was analyzed for absorbance using Cary 60 UV–vis spectrophotometer (Agilent Technologies, UK) to quantify the mass of any uncomplexed myoglobin (510 nm) or eGFP and cGFP (488 nm) (M_s), and to determine the mass of sequestered guest species in the coacervate microdroplets (M_c). The partitioning coefficient was calculated as a ratio of sequestered mass of protein (M_c) to the total mass (M_t) of protein (Equation (2))

$$P = \frac{M_c}{M_t} = \frac{M_t - M_s}{M_t} \quad (2)$$

Zeta Potential: Mean zeta potential of coacervate microdroplets was obtained using ZetaSizer Nano ZS (Malvern Instruments, UK) and analyzed using ZetaSizer software (Malvern Instruments, UK). Zeta potential was measured at 25 °C with 10–100 runs per sample after a 300 s equilibration.

Glass Surface Modification for Imaging: In order to minimize the effect of heavy wetting of coacervate microdroplets on glass surfaces due to their hydrophobic properties, glass surfaces were functionalized with 2-[methoxy(polyethyleneoxy)propyl]trimethoxysilane (m-PEG-TMOS) (ABCR GmbH, Germany). Glass cover slips were bathed in 10 mL fresh 2% PEG-toluene solution for 1 h and the coated glass cover slips were next washed in excess water and air dried.

Coacervate Microdroplet Size: Total volume of 300 µL of coacervate microdroplets was prepared using standard coacervate preparation method, where the coacervate bulk phase was resuspended in 300 µL of Milli-Q water. The resulting microdroplets were deposited on PEG-coated glass cover slips, imaged by acquiring bright field images using a DMI 3000 inverted microscope (Leica, UK) in Wolfson Bioimaging Facility (Medical Sciences, University of Bristol). The image processing and statistical particle size analysis were performed using "analyze particle" tool of Fiji software. 5000 microdroplets were measured for each complex of which an average was determined.

Coacervate Microdroplets Imaging: All microscopy imaging was acquired at the Wolfson Bioimaging Facility (University of Bristol, UK) using a Leica SP8 confocal multilaser scanning coupled with DM I6000 inverted epifluorescence microscope (Leica, UK). Coacervate microdroplets were introduced onto the PEG-coated glass slides and imaged using DAPI fluorophore (ex. 340–380 nm, em. 430–480) for Hoechst, GFP fluorophore (ex. 450–490 nm, em. 510–550) for eGFP, cationized eGFP, and FITC-tagged molecules, and rhodamine fluorophore (ex. 510–560 nm, em. 565–605 nm) for rhodamine-tagged molecules. Images were captured using Leica LAS-X acquisition software (Leica, UK) and processed by Fiji software.

Protein Payload Release: Total volume of 300 µL of coacervate microdroplets was prepared using standard coacervate preparation method, where the coacervate bulk phase was resuspended in 250 µL of Milli-Q water, followed by addition of 50 µL of NaCl (0.0–1.0 M) or 50 µL of α-amylase from *Bacillus amyloliquefaciens* (Sigma-Aldrich, UK) (0.25, 2.5, and 25 units g^{-1}), with an incubation time of 3 and 24 h. The control used 50 µL of Milli-Q water in place of the enzyme.

To quantify the release of eGFP from coacervate microdroplets upon exposure to the factors introduced, samples were centrifuged down to isolate supernatant for analysis with Mithras LB940 multimode microplate reader (Berthold Technologies, UK). Collected fluorescence and absorbance readings were subsequently converted to protein concentrations upon comparison to standard curve.

hMSC Culture: hMSCs were isolated, characterized, cultured, and passaged as previously described.[17]

Cell-Coacervate Microdroplet Interaction Imaging: A Leica SP8 AOBS confocal laser scanning microscope attached to a Leica DM I6000 inverted epifluorescence microscope was used for live-cell imaging. Location of individual components as well as delivered payloads within cells was tracked by incubating hMSCs for 30 min in staining media containing 0.5×10^{-6} M Cell Tracker Red CMTPX (Life Technologies, USA) and Hoechst 33342 (Life Technologies, USA). The excitation filters used were DAPI fluorophore (360/40 nm) for Hoechst, GFP fluorophore (450–490 nm) for cells labeled with the constructs and rhodamine fluorophore (515–560 nm) for cytoplasm. Images were captured using Leica LAS-X acquisition software (Leica, UK) and processed by Fiji software.

Cytoxicity Assays: Viability of hMSCs after exposure to coacervate material was measured by a 3-(4,5-dimethylthiazol-2-yl)-5-(3-carboxymethoxyphenyl)-2-(4-sulfophenyl)-2H-tetrazolium (MTS) assay (Promega, USA). The hMCSs from three patients were plated in triplicates in 96 well plates, with 5000 cells per well, and incubated at 37 °C overnight to adhere. 0, 500, 1000, 2500, 5000, 7500, 10 000, and 15 000 cells were seeded per well under identical conditions for the standard curve. The cells were incubated with coacervate microdroplets for 15 mins at a range of concentrations of 90 (low), 180 (medium), and 1800 (high) microdroplets per cell, in FBS-free media, after which the media with free floating microdroplets was replaced with complete media supplemented with 10% FBS and incubation for a further 4 h. The viability of cells was assessed by replacing the media with 100 µL of phenol-free expansion media and 20 µL of CellTiter 96 AQ One Solution Reagent in each well. Cells were incubated at 37 °C for 3 h, and then 100 µL of supernatant was transferred to a 96 well plate before measuring absorbance at 490 nm using a plate reader (Mithras LB940 plate reader, Berthold Technologies, USA). The number of living cells was converted using standard curve absorbance measurements.

In Vitro Osteogenic Differentiation of hMSCs: 133 000 hMSCs (passage number 1) from three patients were seeded into each well of 6 well plates and were allowed to attach for 24h. 1 µL of 100 µg mL^{-1} BMP2 was added in a total 60 µL of coacervate microdroplets and cells were treated with 1 µL of BMP2 loaded coacervate microdroplets in partial differentiation medium (α-MEM supplemented with $NaHCO_3$, 0.01×10^{-6} M dexamethasone ethanol, 0.25×10^{-3} M ascorbic acid, 0.01 M β-glycerophosphate) for 20 min and the medium was replaced with partial differentiation medium. The positive control groups were exposed to complete differentiation medium of α-MEM supplemented with $NaHCO_3$, 100×10^{-6} M dexamethasone ethanol, 80×10^{-3} M ascorbic acid, 1 M β-glycerophosphate and 100 µg mL^{-1} BMP2. The negative control groups were incubated only in basal medium of α-MEM. The cells were cultured for 1 week with medium change every other day, introducing freshly prepared BMP2-loaded coacervate microdroplets every time.

qPCR: Cells were lysed and total RNA was extracted using RNeasy Micro Kit (Qiangen, Germany), following the manufacturer's instructions. RNA concentration of each sample was assessed using NanoDrop ND2000 (Labtech International, UK), followed by dilution of all samples down to a same concentration of 20 ng µL^{-1} with Easy Dilution Buffer, and addition of megamix (Takara, Japan). cDNA synthesis was performed by reverse transcription at 37 °C for 15 min, followed by inhibition of reverse transcription at 85 °C for 5 s and cooling down to 4 °C, using a Labcycler SensoQuest cycler machine (Geneflow, UK). Finally, cDNA samples were diluted in RNase-free water and added to qPCR wells together with RUNX2 or ALPL and Taqman mastermix (Life Technologies, UK), and compared against a housekeeping gene GAPDH. The gene amplification was conducted using StepOnePlus Real-Time PCR System (Applied Biosystems, USA) with the following steps; polymerase enzyme activation at 95 °C for 10 min and forty cycles of denaturation at 95 °C for 15 s and annealing of primers and extension at 60 °C for 1 min.

ALP Protein Colorimetric Assay: 15 000 hMSCs (passage number 1) from three patients were seeded into each well of 48 well plates for osteogenic differentiation using BMP2 loaded coacervate microdroplets. After a week, ALP protein expression was assessed using an ALP assay kit (GeneTex, UK), following the manufacturer's instructions. The ALP enzyme convert 4-methylumbelliferyl phosphate substrate to equal amount of fluorescent 4-methylumbelliferone (4-MU) and the resulting fluorescence intensity of 4-MU was measured using a plate reader (Biotek, USA) with excitation at 360 nm and emission detection at 440 nm.

Statistical Analysis: Comparison of differences was tested using ANOVA and a two-tailed Student's *t*-test with *p*-value of less than 0.05 and 0.01 considered significant (*) and highly significant (**), respectively. Data presentation and sample size for each study were mentioned in the corresponding figures.

Supporting Information

Supporting Information is available from the Wiley Online Library or from the author.

Acknowledgements

W.X. and M.D.J. contributed equally to this work. The authors would like to acknowledge the Wolfson Bioimaging Centre at the University of Bristol (BBSRC Alert 13 capital grant (BB/L014181/1). The authors thank EPSRC (Doctoral Training Centre Grant EP/G036780/1) for funding M.D.J., the Defence Science & Technology laboratory (DSTL) for funding I.Z., the University of Bristol for funding S.N., and EPSRC (Early Career Fellowship EP/K026720/1) for support of A.W.P. The authors thank the Ser Cymru II programme for support of D.S.W.; this project received funding from the European Union's Horizon 2020 research and innovation programme under the Marie Skłodowska-Curie Grant Agreement No. 663830. Data are available at the University of Bristol data repository, data.bris, at https://doi.org/10.5523/bris.1v7ah03ajjb6o2w1tu9tvmxxu9

Conflict of Interest

The authors declare no conflict of interest.

Keywords

biologics, complex coacervates, drug delivery, microvectors, protein delivery

Received: April 2, 2020
Revised: September 29, 2020
Published online: November 9, 2020

[1] D. W. Long, N. R. Johnson, E. M. Jeffries, H. Hara, Y. Wang, *J. Controlled Release* **2017**, *253*, 73.
[2] X. Li, W. Yang, Y. Zou, F. Meng, C. Deng, Z. Zhong, *J. Controlled Release* **2015**, *220*, 704.
[3] B. Leader, Q. J. Baca, D. E. Golan, *Nat. Rev. Drug Discovery* **2008**, *7*, 21.
[4] A. Mullard, *Nat. Rev. Drug Discovery* **2013**, *12*, 87.
[5] *Haschek and Rousseaux's Handbook of Toxicologic Pathology,* 3rd ed., Academic Press, *USA* **2008**.

[6] F. Sgolastra, C. M. Backlund, E. I. Ozay, B. M. deRonde, L. M. Minter, G. N. Tew, *J. Controlled Release* **2017**, *254*, 131.
[7] M. Yu, J. Wu, J. Shi, O. C. Farokhzad, *J. Controlled Release* **2016**, *240*, 24.
[8] M. C. Koetting, J. F. Guido, M. Gupta, A. Zhang, N. A. Peppas, *J. Controlled Release* **2016**, *221*, 18.
[9] V. R. Sinha, A. Trehan, *J. Controlled Release* **2003**, *90*, 261.
[10] S. Frokjaer, D. E. Otzen, *Nat. Rev. Drug Discovery* **2005**, *4*, 298.
[11] L. R. Brown, *Expert Opin. Drug Delivery* **2005**, *2*, 29.
[12] M. C. Manning, D. K. Chou, B. M. Murphy, R. W. Payne, D. S. Katayama, *Pharm. Res.* **2010**, *27*, 544.
[13] A. C. Anselmo, Y. Gokarn, S. Mitragotri, *Nat. Rev. Drug Discovery* **2019**, *18*, 19.
[14] A. Fu, R. Tang, J. Hardie, M. E. Farkas, V. M. Rotello, *Bioconjugate Chem.* **2014**, *25*, 1602.
[15] W. C. B. McTigue, S. L. Perry, *Soft Matter* **2019**, *15*, 3089.
[16] A. Harada, K. Kataoka, *Macromolecules* **1998**, *31*, 288.
[17] J. P. K. Armstrong, S. N. Olof, M. D. Jakimowicz, A. P. Hollander, S. Mann, S. A. Davis, M. J. Miles, A. J. Patil, A. W. Perriman, *Chem. Sci.* **2015**, *6*, 6106.
[18] A. Harada, K. Kataoka, *Macromolecules* **1995**, *28*, 5294.
[19] T. Trantidou, M. Friddin, Y. Elani, N. J. Brooks, R. V. Law, J. M. Seddon, O. Ces, *ACS Nano* **2017**, *11*, 6549.
[20] N. R. Johnson, Y. Wang, *Expert Opin. Drug Delivery* **2014**, *11*, 1829.
[21] W. C. Blocher, S. L. Perry, *WIREs Nanomed. Nanobiotechnol.* **2017**, *9*, 1442.
[22] J. Zhu, K. Xia, W. Yu, Y. Wang, J. Hua, B. Liu, Z. Gong, J. Wang, A. Xu, Z. You, Q. Chen, F. Li, H. Tao, C. Liang, *Acta Biomater.* **2019**, *86*, 300.
[23] H. Chu, J. Gao, C.-W. Chen, J. Huard, Y. Wang, *Proc. Natl. Acad. Sci. USA* **2011**, *108*, 13444.
[24] H. K. Awada, N. R. Johnson, Y. Wang, *Macromol. Biosci.* **2014**, *14*, 679.
[25] N. R. Johnson, M. Kruger, K. P. Goetsch, P. Zilla, D. Bezuidenhout, Y. Wang, N. H. Davies, *ACS Biomater. Sci. Eng.* **2015**, *1*, 753.
[26] U. Park, M. S. Lee, J. Jeon, S. Lee, M. P. Hwang, Y. Wang, H. S. Yang, K. Kim, *Acta Biomater.* **2019**, *90*, 179.
[27] S. L. Perry, Y. Li, D. Priftis, L. Leon, M. Tirrell, *Polymers* **2014**, *6*, 1756.
[28] J. R. Vieregg, M. Lueckheide, A. B. Marciel, L. Leon, A. J. Bologna, J. R. Rivera, M. V. Tirrell, *J. Am. Chem. Soc.* **2018**, *140*, 1632.
[29] M. G. F. Last, S. Deshpande, C. Dekker, *ACS Nano* **2020**, *14*, 4487.
[30] S. Mizrahy, D. Peer, *Chem. Soc. Rev.* **2012**, *41*, 2623.
[31] H. J. Prado, M. C. Matulewicz, *Eur. Polym. J.* **2014**, *52*, 53.
[32] A. F. Mason, N. A. Yewdall, P. L. W. Welzen, J. Shao, M. van Steve ndaal, J. C. M. van Hest, D. S. Williams, L. K. E. A. Abdelmohsen, *ACS Cent. Sci.* **2019**, *5*, 1360.
[33] A. F. Mason, B. C. Buddingh, D. S. Williams, J. C. M. van Hest, *J. Am. Chem. Soc.* **2017**, *139*, 17309.
[34] E. Amar-Lewis, A. Azagury, R. Chintakunta, R. Goldbart, T. Traitel, J. Prestwood, D. Landesman-Milo, D. Peer, J. Kost, *J. Controlled Release* **2014**, *185*, 109.
[35] D. S. Williams, S. Koga, C. R. C. Hak, A. Majrekar, A. J. Patil, A. W. Perriman, S. Mann, *Soft Matter* **2012**, *8*, 6004.
[36] S. Lindhoud, R. de Vries, W. Norde, M. A. C. Stuart, *Biomacromolecules* **2007**, *8*, 2219.
[37] S. Lindhoud, M. M. A. E. Claessens, *Soft Matter* **2015**, *12*, 408.
[38] A. C. Obermeyer, C. E. Mills, X.-H. Dong, R. J. Flores, B. D. Olsen, *Soft Matter* **2016**, *12*, 3570.
[39] K. A. Black, D. Priftis, S. L. Perry, J. Yip, W. Y. Byun, M. Tirrell, *ACS Macro Lett.* **2014**, *3*, 1088.
[40] U. B. Hendgen-Cotta, U. Flögel, M. Kelm, T. Rassaf, *J. Exp. Biol.* **2010**, *213*, 2734.
[41] J. P. K. Armstrong, R. Shakur, J. P. Horne, S. C. Dickinson, C. T. Armstrong, K. Lau, J. Kadiwala, R. Lowe, A. Seddon, S. Mann, J. L. R. Anderson, A. W. Perriman, A. P. Hollander, *Nat. Commun.* **2015**, *6*, 7405.
[42] S. Barthold, S. Kletting, J. Taffner, C. de, S. Carvalho-Wodarz, E. Lepeltier, B. Loretz, C.-M. Lehr, *J. Mater. Chem. B* **2016**, *4*, 2377.
[43] L.-P. Bergeron-Sandoval, H. K. Heris, C. Chang, C. E. Cornell, S. L. Keller, P. François, A. G. Hendricks, A. J. Ehrlicher, R. V. Pappu, S. W. Michnick, *bioRxiv* **2018**, https://doi.org/10.1101/145664.
[44] M. Phimphilai, Z. Zhao, H. Boules, H. Roca, R. T. Franceschi, *J. Bone Miner. Res.* **2006**, *21*, 637.
[45] Y.-J. Kim, M.-H. Lee, J. M. Wozney, J.-Y. Cho, H.-M. Ryoo, *J. Biol. Chem.* **2004**, *279*, 50773.
[46] E. Ragni, M. Viganò, P. Rebulla, R. Giordano, L. Lazzari, *J. Cell. Mol. Med.* **2013**, *17*, 168.
[47] A. von Bubnoff, K. W. Y. Cho, *Dev. Biol.* **2001**, *239*, 1.
[48] A. Rutkovskiy, K.-O. Stensløkken, I. J. Vaage, *Med. Sci. Monit. Basic Res.* **2016**, *22*, 95.
[49] W. Huang, S. Yang, J. Shao, Y.-P. Li, *Front. Biosci.* **2007**, *12*, 3068.
[50] B. Kulterer, G. Friedl, A. Jandrositz, F. Sanchez-Cabo, A. Prokesch, C. Paar, M. Scheideler, R. Windhager, K.-H. Preisegger, Z. Trajanoski, *BMC Genomics* **2007**, *8*, 70.
[51] P. Müller, U. Bulnheim, A. Diener, F. Lüthen, M. Teller, E.-D. Klinkenberg, H.-G. Neumann, B. Nebe, A. Liebold, G. Steinhoff, J. Rychly, *J. Cell. Mol. Med.* **2008**, *12*, 281.
[52] O. Jeon, D. W. Wolfson, E. Alsberg, *Adv. Mater.* **2015**, *27*, 2216.